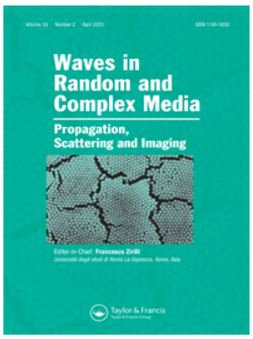

Taylor & Francis
Taylor & Francis Group

Waves in Random and Complex Media

ISSN: (Print) (Online) Journal homepage: https://www.tandfonline.com/loi/twrm20

Switching of electromagnetically induced transparency and absorption of graphene metastructure with the three resonators

Di-Di Zhu, You Lv, Yuan-Zhe Sun & Hai-Feng Zhang

To cite this article: Di-Di Zhu, You Lv, Yuan-Zhe Sun & Hai-Feng Zhang (2023): Switching of electromagnetically induced transparency and absorption of graphene metastructure with the three resonators, Waves in Random and Complex Media, DOI: 10.1080/17455030.2023.2182142

To link to this article: https://doi.org/10.1080/17455030.2023.2182142

Published online: 28 Apr 2023.

WAVES IN RANDOM AND COMPLEX MEDIA
https://doi.org/10.1080/17455030.2023.2182142

Taylor & Francis
Taylor & Francis Group

Switching of electromagnetically induced transparency and absorption of graphene metastructure with the three resonators

Di-Di Zhu, You Lv, Yuan-Zhe Sun and Hai-Feng Zhang

College of Electronic and Optical Engineering & Flexible Electronics (Future Technology) of Microelectronics, Nanjing University of Posts and Telecommunications, Nanjing, People's Republic of China

ABSTRACT

A graphene metastructure (GMST) with switching features from electromagnetically induced transparency (EIT) and absorption (EIA) is theoretically proposed in a three-resonator system by controlling the Fermi energy (Ef) of the graphene in the terahertz (THz) regime. When Ef = 0.9 eV, the graphene has less influence on the lower EIT metastructure, and the EIT phenomenon of the three-resonator metastructure is realized. The EIT transmission window appears between 0.763 and 0.965 THz, and at 0.803 THz, the transmission peak reaches 0.860. When Ef = 0.12 eV, graphene is weakly coupled to the substructure, thus constructive interference between the three resonators generates a magnetic dipole that strongly traps the incident magnetic energy, thus contributing to the EIA phenomenon. The absorption window appears between 0.650 and 0.902 THz. The frequency point of the absorption peak of the EIA phenomenon at this time coincides perfectly with the frequency point of the transmission peak of EIT at Ef = 0.9 eV, both at 0.803 THz. The working principle of this GMST is explained through the surface current distribution. To reproduce EIT and EIA, the two oscillator model is used and the simulation results are proved to be consistent and valid. The structural parameters are also discussed and the properties of the GMST are explored.

ARTICLE HISTORY
Received 15 September 2022
Accepted 13 February 2023

KEYWORDS
Electromagnetically induced transparency; electromagnetic induced absorption; graphene; metastructure; two-oscillator model

1. Introduction

Terahertz (THz) technology has abundant characteristics, such as broadband [1], low-energy [2], high-resolution [3] and coherence [4]. Therefore, THz technology has become a hot research topic nowadays [5]. In recent years, the rise of the so-called metastructures [6], that is, metamaterials and metasurfaces, have unique and exotic physical properties compared with natural materials, such as negative refraction, and negative permittivity [7]. It has become the 'favorite' of numerous laboratories. Using its distinctive electromagnetic properties, metastructures can be controlled effectively and further the propagation of electromagnetic waves can be controlled [8]. As the basis of wave-functional

CONTACT Hai-Feng Zhang hanlor@163.com

materials and fluctuation phenomena, electromagnetic resonance can make some periodically arranged unitary structures manifest many exotic electromagnetic properties, which are widely used in the research of electromagnetic induced transparency (EIT) [9,10].

EIT originally refers to the emergence of a narrow band of transmissive frequency bands in an atomic system [11] through the coherent action of a coupled beam in a medium that is initially impermeable to waves. EIT is accompanied by important consequences, such as a significant reduction in group velocity and enhanced nonlinear interactions [12]. These properties lead to a wide range of applications for EIT in areas such as slow light, optical signal processing, quantum switching, and four-wave mixing [13,14]. However, the generation of EIT requires harsh conditions such as ultra-low temperature, which greatly limit EIT applications [15]. To realize miniaturized and multifunctional metastructure devices based on EIT effects in practical applications, mimicking quantum phenomena in metastructure by coupling classical resonators has attracted great interest from researchers. The ability to overcome the harsh conditions of low temperature is required to realize EIT in atomic systems. The first successful realization of EIT behavior through electromagnetic metastructure was achieved by Zhang et al. in 2008 [16]. Since then, experimenting with EIT using metastructure has become a common phenomenon. The first method is achieved by frequency detuning and weak hybridization between two bright-mode resonators [17]. Under the action of incident light, both resonators are excited, resulting in a sharp transmission window [18,19]. The second method is achieved by phase destructive interference between bright-mode and dark-mode resonators [20,21], where the bright-mode is directly excited by the resonance of the incident light to produce electrical resonance [22], while the dark-mode cannot, and it needs to be coupled by the bright-mode resonator near-field to produce magnetic resonance [23].

Distinguished from the phase destructive interference between coupled resonators that realize EIT, the phase constructive interference of different excitation paths may result in a new magical effect, namely, electromagnetic induced absorption (EIA) [24]. Although EIT has been fruitfully studied in metastructure systems, the study of EIA is still in the process of development [25]. According to the prediction, EIA will open new paths in the design of new photonic devices for narrowband filtering, absorption switching, and optical modulators [24]. Several groups have reported that the transition from EIT to EIA can be observed in two-resonator system metastructures by reducing the dissipation loss of the bright mode [26,27], increasing the dissipation loss of the dark mode [28], or reducing the coupling strength between the bright-mode and dark-mode(e.g. by increasing the coupling distance)[29], as well as by different phases involved in the oblique incidence [30]. In addition, the EIA can be achieved in a three-resonator metastructure by adding a resonator in a way that generates interference between more than three excitation paths [25]. Erçağlar et al. in 2017 [31] utilized the VO_2 phase change property to realize bi-tunable phonon-induced transparency and resonant absorption. The essence is the narrow-band absorption formed by reducing electromagnetic wave transmission and increasing reflection through metallic VO_2, rather than EIA. In practice, active manipulation of EIT resonances is highly desired as it helps a lot in transferring additional dimensions of the design and functionality of the metastructure. Lately, introducing active materials into the metastructure cells has been reported as a way to achieve dynamically controllable EIT resonance [25]. Graphene is an electric control material that is increasingly becoming a 'star material'

in the field of metastructures by virtue of its conductivity that can be continuously adjusted by controlling the Fermi energy(E_f) level with an applied voltage. Graphene provides a tremendous platform for active modulation of EIT [31]. The study of EIT and EIA is a hot topic today. However, fewer integrate these two effects in a single metastructure. Let alone the active modulation of the metastructure. Until now, numerous EIT/EIA metastructure configurations are widely discussed, but fewer pour attention to the combination and autoswitching of both in one device. EIT/EIA metastructure can generate an absorption band in the original EIT transmission window, which opens a new way for advanced information coding technology, decoding and decoding technology, and frequency selection technology.

In this paper, a graphene metastructure(GMST) with switching features from EIT to EIA is theoretically investigated in a three-resonator system by controlling the Ef of the graphene in the terahertz (THz) regime. When $E_f = 0.9$ eV, the graphene has less influence on the lower EIT metastructure, and the EIT phenomenon of the triple-resonator metastructure is realized. The EIT transmission window appears between 0.763 and 0.965 THz, and at 0.803 THz, the transmission peak reaches 0.860. The maximum group delay value is 447 ps, corresponding to a group index of 2410, showing a significant slow light effect. When $E_f = 0.12$ eV, graphene has a certain conductivity and is weakly coupled to the substructure, thus constructive interference between the three resonators generates a magnetic dipole that strongly traps the incident magnetic energy, thus contributing to the EIA phenomenon. The absorption window appears between 0.650 and 0.902 THz. The frequency point of the absorption peak of the EIA phenomenon at this time coincides perfectly with the frequency point of the transmission peak of EIT at $E_f = 0.9$ eV, both at 0.803 THz. In addition, the working principle of this GMST is explained through the surface current distribution. To reproduce EIT and EIA, the two-oscillator model is used and the simulation results are proved to be consistent and valid. The structural parameters are also discussed and the properties of the GMST are explored.

2. Unit design and discussion

2.1. GMST design

Figure 1(a) clearly shows the functions realized by this GMST, through which the incident linearly polarized wave can produce two different states, one for EIT and one for EIA. A view of the proposed GMST cell structure of the given metastructure is shown in Figure 1(b) and (c). The proposed GMST consists of a three-layer dielectric substrate and three resonators. The three layers of dielectric substrate are chosen from plexiglas, the dielectric constant ϵ is 24 [32]. The thicknesses of the three media substrates respectively are $H_1 = 15$ μm, $H_3 = 20$ μm, and $H_5 = 20$ μm. The top view for EIT metastructure and a graphene square patch (GSP) are shown in Figure 1(d) and (e). In EIT metastructure, two cut wires are placed on a plexiglas dielectric substrate, the material selected gold, and the length and width are $D_8 = 130.0$ μm, $W_6 = 25.0$ μm. The middle one is made of two split ring resonators (SRRs), with the same structure, opposite openings and mirror symmetry to each other, and the material chosen is gold. The thicknesses of both resonators are 0.3 μm. The conductivity is 4.1×10^7 S/m [14] for all the gold in the GMST. The GSP with side length $L_5 = L_6 = 39.8$ μm is placed on the second dielectric substrate, and the E_f of graphene is changed by

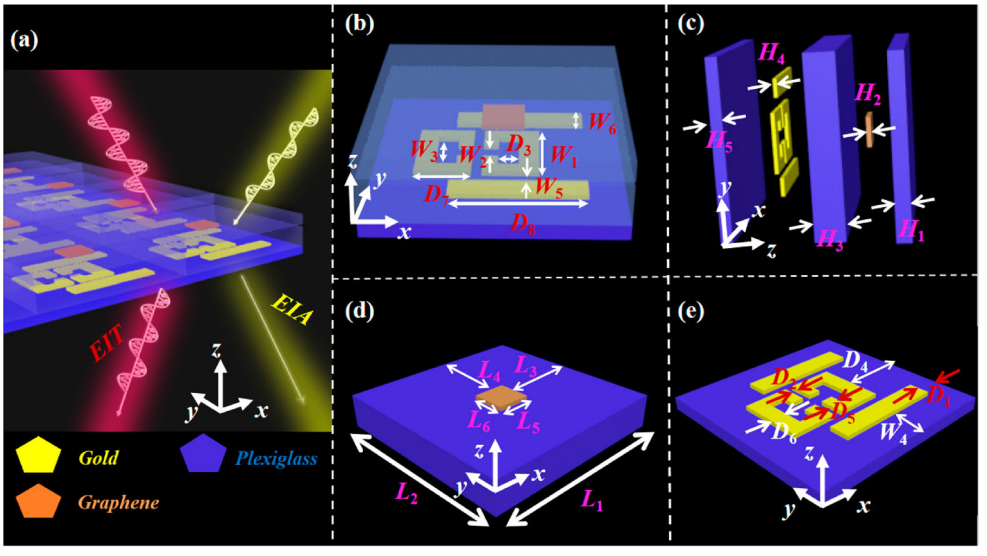

Figure 1. (a) The two modes of the proposed GMST, (b) Top view for EIT metastructure, (c) The stereogram of the cell metastructure, (d) Top view for EIT metastructure, and (e) Top view for GSP.

Table 1. Detailed dimensions.

Parameters	H_1	H_2	H_3	H_4	H_5	D_1	D_2
Value (μm)	15	0.1[33]	20	0.3	20	35.0	10.0
Parameters	D_3	D_4	D_5	D_6	D_7	D_8	W_1
Value (μm)	20.0	80.0	15.0	20.0	55.0	130.0	80.0
Parameters	W_2	W_3	W_4	W_5	W_6	L_1	L_2
Value (μm)	20.0	20.0	41.0	14.0	25.0	240.0	240.0
Parameters	L_3	L_4	L_5	L_6			
Value (μm)	100.0	102.2	39.8	39.8			

controlling the external bias voltage to further change the conductivity as well as the dielectric loss of graphene. The thickness of the GSP is designed as $H_2 = 0.1$ μm [33]. Detailed geometrical dimensions are shown in Table 1.

The dynamic surface conductivity $\sigma_g(\omega)$ of graphene in the low THz range can be calculated using the Kubo formula [34]. $\sigma_g(\omega)$ of graphene consists of two components, intra-band conductivity $\sigma_{\text{intra}}(\omega)$ and inter-band conductivity $\sigma_{\text{inter}}(\omega)$ [32]

$$\sigma_g(\omega) = \sigma_{\text{intra}} + \sigma_{\text{inter}} \tag{1}$$

Among them [32]:

$$\sigma_{\text{intra}}(\omega) = \frac{-je^2 k_b T}{\pi\hbar^2(\omega + 2j\tau)}\left(\frac{\mu_c}{k_b T} + 2\ln(e^{\frac{\mu_c}{k_b T}} + 1)\right) \tag{2}$$

$$\sigma_{\text{inter}}(\omega) = \frac{-je^2}{4\pi\hbar}\ln\left(\frac{2\mu_c - (\omega + 2j\Gamma)\hbar}{2\mu_c + (\omega + 2j\Gamma)\hbar}\right) \tag{3}$$

where ω is the radian frequency of the incident THz wave, e is the charge of an electron, k_B is the Boltzmann constant, $\hbar$ is the reduced Planck's constant and $\hbar = h/(2\pi)$. Moreover, Γ

and T are chosen to be 0.43 meV [35] and 300 K. On the other hand, the surface impedance of graphene is calculated as $Z_G(\omega) = 1/\sigma_g(\omega)$. In general, the interband conductivity of graphene is negligible [36], so the surface conductivity of graphene can be simplified to Drude's model [32]:

$$\sigma_g(\omega) \approx \frac{e^2\mu_c}{\pi t^2}\frac{j}{\omega + j/\pi} \tag{4}$$

Therefore, the surface conductivity of graphene can be adjusted by changing its E_f. The relationship between E_f of graphene and the applied bias voltage. The relationship between E_f of graphene and the applied bias voltage is as follows [37]

$$\mu_c \approx \hbar V_f \sqrt{\frac{\pi\varepsilon_0\varepsilon_r V_g}{et}} \tag{5}$$

where $V_f = 1.1 \times 10^6$ m/s is the Fermi velocity, t is the thickness of the dielectric layer, V_g is the applied bias voltage, ϵ_0 and ϵ_r are the dielectric constants of the vacuum and dielectric layers, respectively.

It is worth emphasizing that this research work is theoretical and the experiments are beyond the scope of our research. But our data are all guaranteed, the model was built and the data results were obtained with the help of the commercial simulation software High Frequency Simulation Software 15.0 (HFSS). The unit cell boundary condition is set along the x- and y-axis directions, the open (add space) boundary condition is set along the z-axis direction, and the electromagnetic wave with polarization direction along the x-axis is incident on the super-surface along the z-axis direction. Use the default adaptive mesh profiling settings. The proposed GMST is based on the TM waves incidence (electric field direction along x-direction, magnetic field direction along y-direction, wave vector direction along z-direction). However, the proposed GMST can be fabricated, and the specific processing can be found in Refs. [38–41].

2.2. EIT mechanism analysis

The metastructure that produces the EIT phenomenon is two cut wires and a resonator consisting of two SRRs. The reason for using two SRRs is that the charge accumulation in a single SRR will produce an electric dipole moment, which weakens the desired electromagnetic moment. The electric dipole moments produced by two SRRs placed with opposite openings will cancel each other out. When the direction of incident electric field is x-direction (the same as the radial direction of the cut wire), it will make both sides of the cut wires the bright mode directly excited to produce electric resonance. As shown in Figure 2(a), this mode is stronger coupled with the free space, and the resulting radiation loss is relatively large. Also known as the electric dipole mode, which shows a wider spectrum and a smaller Q value [15] in the transmission spectrum. The energy of the electric resonance is coupled to two SRRs that cannot be excited by the incident electric field, resulting in magnetic resonance, which is also called dark mode. Figure 2(b) shows the resonance curve of the dark mode excited alone (the direction of the incident magnetic field is perpendicular to plane where dark mode is located). As seen in Figure 2(c), the bright and dark mode resonators satisfy the conditions for EIT generation, namely, the Q difference between electric and magnetic resonance is large and the resonant frequency points are similar (0.976

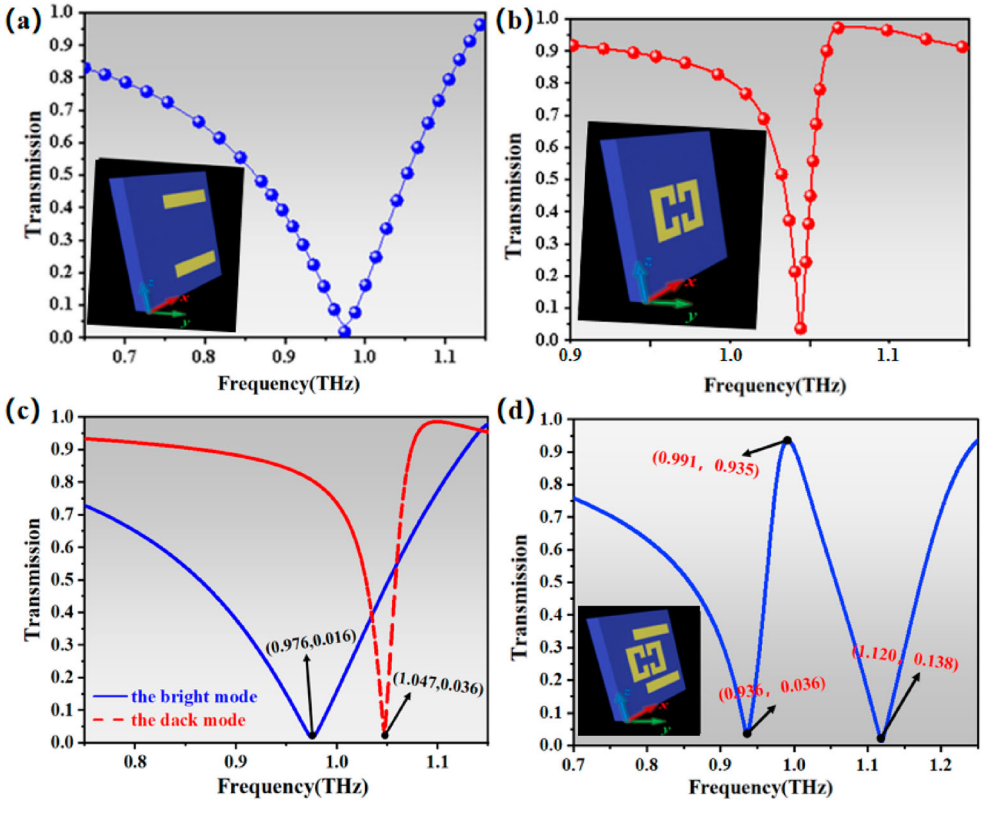

Figure 2. (a) The bright mode being separately excited, (b) The dark mode being separately excited, (c) Bright and dark modes separately excited, and (d) The resulting EIT transmission curve.

and 1.047 THz, respectively). Therefore, When TM waves are incident, the phase destructive interference between electric and magnetic resonance leads to the EIT in Figure 2(d), the metastructure produces transmission valleys at the frequencies of 0.936 and 1.120 THz. and a transmission peak at the frequency of 0.991 THz. The resonant frequencies of the two resonant units are very close to the two resonant frequencies of the complete metastructure, and the transmission peak of the complete structure is in between the two resonant frequencies, which is formed by the weak coupling between the two modes excited by the incident wave. It is shown that the transmission size can be changed by breaking the symmetry of the EIT structure. Therefore, after simulation comparison, the final light and dark mold center offset is designed to be 40 μm. At this point, the transmission peak reaches 0.935.

To illustrate this phenomenon, we start our analysis by discussing the GMST resonants behavior at TM-incidence. In Figure 3, the transmission response of the GMST at TM-incidence is simulated and plotted. As shown in Figure 3(a), the low transmission dip ($f_1 = 0.936$ THz), two cut wires are directly excited to form an electric resonance. The surface current forms a dipole current symmetrical to the upper and lower directions about the middle horizontal line, and the current intensity is strong, forming an electric dipole resonance, which can form a strong coupling with the incident wave (electric direction), and

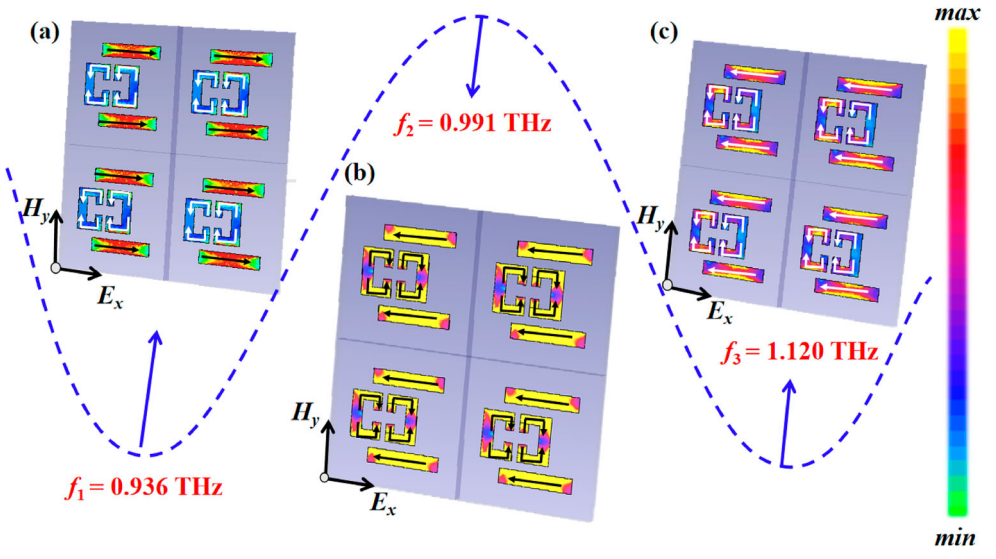

Figure 3. Surface current and electric field diagram of the transmission response of a super-surface at TM-incidence: (a) The low transmission dip ($f_1 = 0.936$ THz), (b) The transmission peak ($f_2 = 0.991$ THz), and (c) The high transmission dip ($f_3 = 1.120$ THz).

the electromagnetic wave loss is large and belongs to the bright mode. And there is almost no current on the SRRs at this time. Figure 3(c) that the high transmission dip ($f_3 = 1.120$ THz) is a symmetric mode. The upper cut wire (lower cut wire) and the current direction on the upper surface of the SRRs (lower surface of the SRRs) coincide, further increasing the electromagnetic radiation loss of the structure. That is, the bandwidth at the high transmission dip is greater than that at the low transmission dip. Figure 3(b) depicts the current distribution at the transmission peak ($f_2 = 0.991$ THz) of the metastructure. As shown, antisymmetric electric field appears on the upper cut wire (lower cut wire) and on the upper surface of SRRs (lower surface of SRRs), and since the current distributions are essentially the same in size and opposite in direction, their resulting radiated electromagnetic fields, i.e. reflected fields, cancel each other out, and the radiation loss of the metastructure at this point is significantly reduced, ultimately leading to the EIT phenomenon. This interesting phenomenon can also be well explained by using the method of equipartition exciton hybridization [38,39]. When the lengths of the uppercut wire (lower-cut wire) and the upper surface of SRRs (lower surface of SRRs) are different, the coupling between them leads to the formation of two plasma exciting modes: antisymmetric and symmetric plasma exciton modes [42]. The antisymmetric and symmetric modes correspond to the currents in the upper cut wire (lower cut wire) and the upper surface of SRRs (lower surface of SRRs), which flow in opposite and the same direction, respectively, as shown in Figure 3(b).

2.3. The physical mechanism of the EIT behavior

To explain the formation of the EIT effect, we can represent it in the typical three-energy Λ-type system [43] shown in the figure below, EIT behavior is realized by the interference

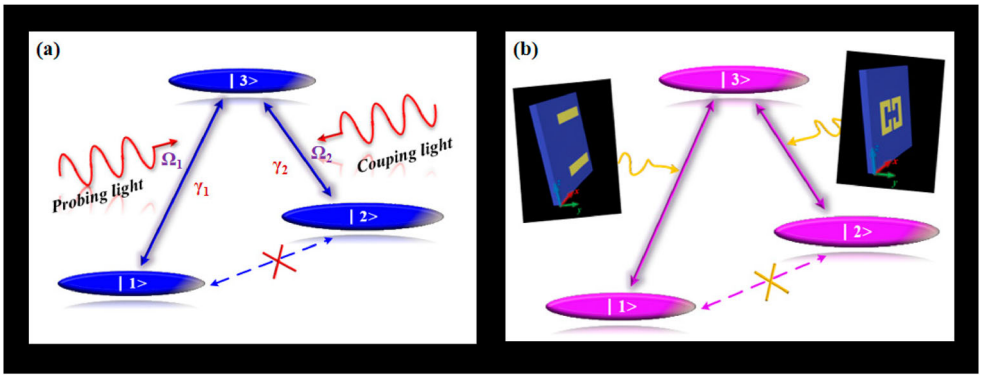

Figure 4. The comparison of the coupling mechanism between: (a) The classical three-level atomic system, and (b) The proposed EIT metastructure.

of two different stimulus paths in the three-level atomic system, which can be used to elaborate the EIT effect. This is shown in Figure 4(a) where γ_1 and γ_2 are the coupling coefficients between the energy levels, Ω_1, and Ω_2 are the transition phases, and $|1>$ and $|2>$ are the ground state energy levels. These two energy levels are similar in energy and are simplicial energy levels, $|3>$ belongs to the excited state energy level, and the jump from $|1>$ energy level to $|2>$ energy level is forbidden. First, the emission of weak-energy electromagnetic waves to detect the absorption of light by the medium, the photon energy of the detected electromagnetic waves and $|1>$ jump to $|3>$ energy approximation. Another beam of electromagnetic waves incident on the medium is a very high energy pump electromagnetic waves, able to couple $|2>$ energy level and $|3>$ energy level, these two beams of electromagnetic waves to meet the resonance conditions, the detection of light will be able to 'transparent' through the medium without being absorbed. In this process, there are two paths from energy level $|1>$ to energy level $|3>$: $|1> \rightarrow |3>$ and $|1> \rightarrow |3> \rightarrow |2> \rightarrow |3>$, and the magnitudes of the odds ratios of these two paths are approximately equal, while the directions are opposite, so that interference effects occur at energy level $|3>$, making the atomic Bourget number at energy level $|3>$ close to 0, and the detection light is no longer absorbed, resulting in electromagnetic-induced transparency [40]. Accordingly, the transition from $|1>$ to $|3>$ is equivalent to the cut wires in Figure 4(b). Meanwhile, the other transition from $|3>$ to $|2>$ is similar to the two SRRs in Figure 4(b). Thus, at TM incident, a high transmittance transparent window is observed when the cut wires are combined with the two SRRs.

Furthermore, to more quantitatively clarify the mechanism of EIT generation, a two-oscillator model is applied to reproduce this EIT metastructure [33,44]. The model diagram is shown in Figure 5(a), where two oscillators of masses m_1 and m_2 are connected by springs with elastic coefficients K and are connected to the wall on the side by two springs with elastic coefficients k_1 and k_2, respectively. Moreover, oscillator 1 is subjected to a simple harmonic force E. Oscillator 1, due to the displacement change by the direct force, corresponds to the bright-mode resonant element in the system with its resonant frequency ω_1, and oscillator 2 equals the dark-mode resonant element with its resonant frequency ω_2. The spring with an elasticity factor k between oscillators 1 and 2 corresponds to the applied pump light in the atomic system, while the model for detecting light in the atomic system

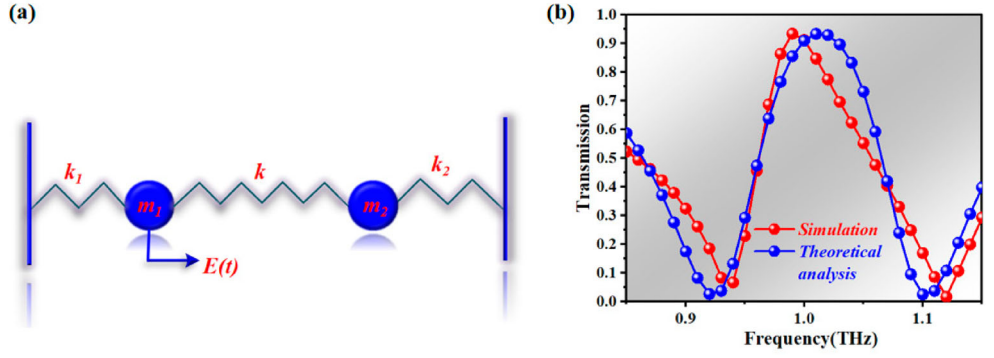

Figure 5. (a) Two-oscillator model, and (b) Comparison of the simulated and theoretical transmission curves of the proposed EIT metastructure.

is the simple harmonic force acting on oscillator 1. To simplify the model, we assume that the oscillators have the same mass and the elasticity coefficients of the springs on both sides are equal, i.e. $m_1 = m_2$ and $k_1 = k_2$. When the electric field $E = E_0 e^{j\omega t}$ is incident, the two oscillators can interact with the electric field, and the interaction can be quantitatively described as follows [15]:

$$x_1''(t) + \gamma_1 x_1'(t) + \omega_0^2 x_1(t) + \Omega^2 x_2(t) = gE \tag{6}$$

$$x_2''(t) + \gamma_2 x_2'(t) + (\omega_0 + \delta)^2 x_2(t) + \Omega^2 x_1(t) = gE \tag{7}$$

To solve the above coupling equations (6) and (7), the displacement vector $x_n = c_n e^{j\omega t}$ $(n = 1,2)$ and $\omega_1^2 - \omega^2 \approx -2\omega_1(\omega - \omega_1)$ [44,45] are introduced. The corresponding transmission can be written as a frequency function as [15]:

$$T = 1 - \mathrm{Re}\frac{ig^2(\omega - \omega_0 - \delta + i\gamma_2/2)}{(\omega - \omega_0 + i\gamma_1/2)(\omega - \omega_0 - \delta + i\gamma_2/2) - \Omega^2/4} \tag{8}$$

Here, the scattering parameters of the current sheet and $T = 1 - R$ are used [46]. We carefully fitted the simulated transmission curves, as shown in Figure 5(b). Finally, the following key fitted parameters $\gamma_1 = 1.18$, $\gamma_2 = 0.07$, $\Omega = 1.111$ and $\omega_0 = 6.368$ were obtained. Figure 5(b) shows a plot of the simulated versus theoretical transmission curves. It is clearly visible that the theoretical results agresses with the simulated results well, which confirms the validity and reasonableness of the given two-oscillator model. In addition, we have to admit that there is a slight mismatch between the two curves. This phenomenon appears mainly due to certain losses and complex coupling generated in the design.

2.4. Mechanistic analysis of EIT to EIA model

The EIT phenomenon originates from the constructive interference of different excitation paths. On the contrary, if these paths interact constructively with each other, the enhanced absorption peak at the resonance frequency will replace the narrow absorption dip accordingly, which allows a perfect conversion of EIT to EIA. In four-energy atomic systems, the conditions for conversion are more demanding and the regulation of each

relevant parameter change is difficult. The first experimental demonstration of EIA occurring in atomic systems was done by the Akulshin group [47]. However, the implementation in the classical oscillator model seems to be much simpler: we can achieve whether they are amplitude-strengthened or amplitude-diminished by simply adjusting the oscillator phase to transform the phase destructive interference between them into a phase constructive interference. As for the design of the metastructure simulated EIT to EIA in this paper, according to several sets of studies, in the dual resonator system metastructure, by reducing the dissipation loss of the bright resonant and increasing the dissipation loss of the dark resonant (e.g. the materials of the dual resonator are chosen to be metallic and dielectric to increase the loss difference, respectively), or by reducing the coupling strength between the bright and dark resonants (e.g. increasing the coupling distance), and the oblique incidence involved different angles involved, a shift from EIT to EIA can be observed[24,26–30]. However, the transition from EIT to EIA, which is generally achieved in two-resonator systems, cannot be actively regulated and both phenomena cannot be achieved in one metastructure. Therefore, graphene is introduced into the structure as the third resonator in the original two-resonator EIT structure, and the property is used that graphene can dynamically adjust the conductivity by changing the E_f to realize the switchable EIT and EIA functions in the GMST.

A dielectric substrate with a thickness of 20 μm is added on top of the original two-resonator EIT metastructure, which material is plexiglas, to place a GSP with an edge length of 39.8 μm as the third resonator layer and precisely set the optimal graphene position (as can be seen in Figure 6(d)). And a layer of dielectric substrate with a thickness of 15 μm is placed at the top, which material is plexiglas. As shown in Figure 6(a) and (c), when two layers of dielectric substrate were added on top of the original two-resonator EIT metastructure, the transmission curve showed a red-shift phenomenon. Subsequently, the GSP is added, and considering the property that the dielectric loss of graphene decreases with the increase of E_f, $E_f = 0.9$ eV is set at this time, and compared with Figure 6(a) and (b), although the conductivity of graphene is high at this time, because of its low dielectric loss, small shape and small coupling with the lower two-resonator EIT metastructure, and the precise setting of the interference position leads to the small effect of graphene on the EIT phenomenon. The transmission curve is slightly red-shifted and the peak is slightly sacrificed. Thus, since the newly introduced GSP does not work when $E_f = 0.9$ eV, a perfect EIT phenomenon can still be observed in the triple-resonator metastructure.

When $E_f = 0.12$ eV, GSP has a certain permeability as well as a large dielectric loss, at this time, due to the magnetic resonance generated by the near-field coupling of the three resonators, the enhanced absorption peak at the resonant frequency will replace the narrow absorption dip accordingly, and a good absorption resonance is formed in the EIT window, thus realizing the transition from phase destructive interference to phase length interference. As shown in Figure 7(a) and (b), this EIT and EIA function switchable metastructure forms EIT phenomenon at $E_f = 0.9$ eV, the transmission interval lies between 0.763 and 0.965 THz, and when the transmission peak reaches 0.860, the transmission peak lies at 0.803 THz. The EIA phenomenon is formed when $E_f = 0.12$ eV and a very clear absorption peak at 0.803 THz can be seen in Figure 7(c) and (d), which coincides perfectly with the EIT transmission peak. The absorption at this frequency is fully promoted by the incident field and its absorption exceeds 52%, which means that the absorption is greatly promoted at this frequency point. However, in the frequency range outside the absorption region,

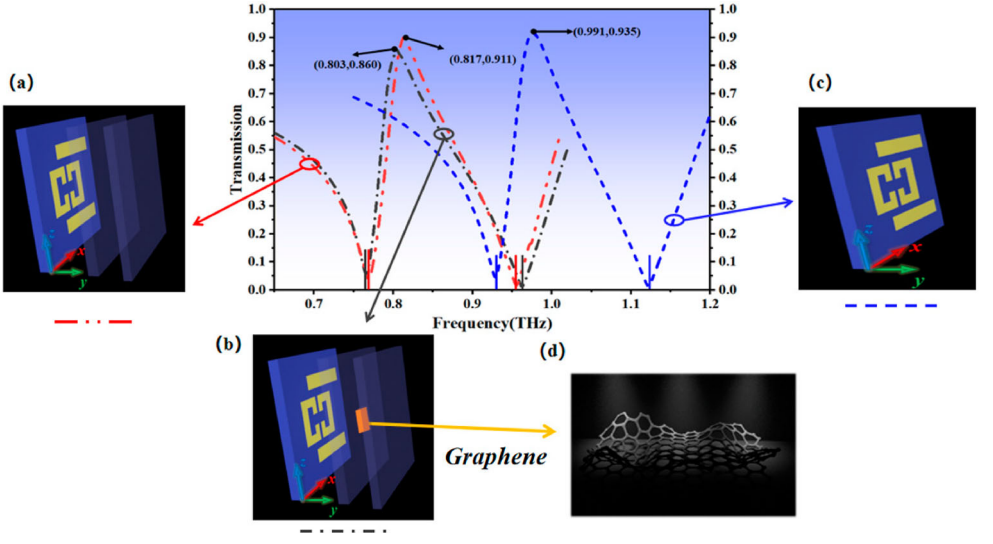

Figure 6. Comparison of transmission curves in three modes, (a) Dual-resonator EIT structure plus two layers of dielectric substrate, (b) Triple-resonator EIT structure (at this time the graphene E_f is set to 0.9 eV), (c) Dual-resonator EIT metastructure, and (d) The view of the graphene.

the absorption is almost always close to 0. This means that the phase delay at this frequency point is well-matched and therefore phase constructive interference is successfully obtained, while the rest of the frequency range fails to obtain phase delay matching and therefore the absorption is close to 0.

To elucidate the physical processes involved, the GMST surface current distribution is calculated. Figure 7 shows the simulated surface current distribution with a phase difference in the GMST, and Figure 7(c) shows the case at peak absorption frequency when $\varphi = 0.89\,\pi$. while Figure 7(d) shows the same frequency when $\varphi = 1.89\,\pi$. A closer look at Figure 7(c) and (d) yields that there is a π-phase difference between the GSP and the two SRRs at TM-incidence, and the reverse current between the two resonators forms a magnetic dipole, the ring shape is indicated by the red line. From the right-hand rule, we can tell that the magnetic dipole direction m is along the *y*-axis, which is the same direction as the incident magnetic field polarization[25,48]. Therefore, it strongly captures the incident magnetic energy, which causes strong absorption[25]. Therefore, the coupling effect (e.g. phase difference) between resonators is changed by adding a third resonator in such a way that the interference path is increased to transform the phase destructive interference between them into phase constructive interference. A deeper understanding of the underlying coupling mechanism can not only provide remarkable insight into the design and optimization of metastructures with the desired functionality but also lead to many fascinating phenomena.

It can also be understood that the original two-resonator EIT metastructure achieves an abnormal enhancement of the electric field, and then a GSP is placed above the metastructure to localize the energy. Due to the dielectric loss in graphene and the impedance matching at resonance, a very strong absorption will occur at the electric field enhancement. When a beam of electromagnetic waves comes into contact with a material, to effectively

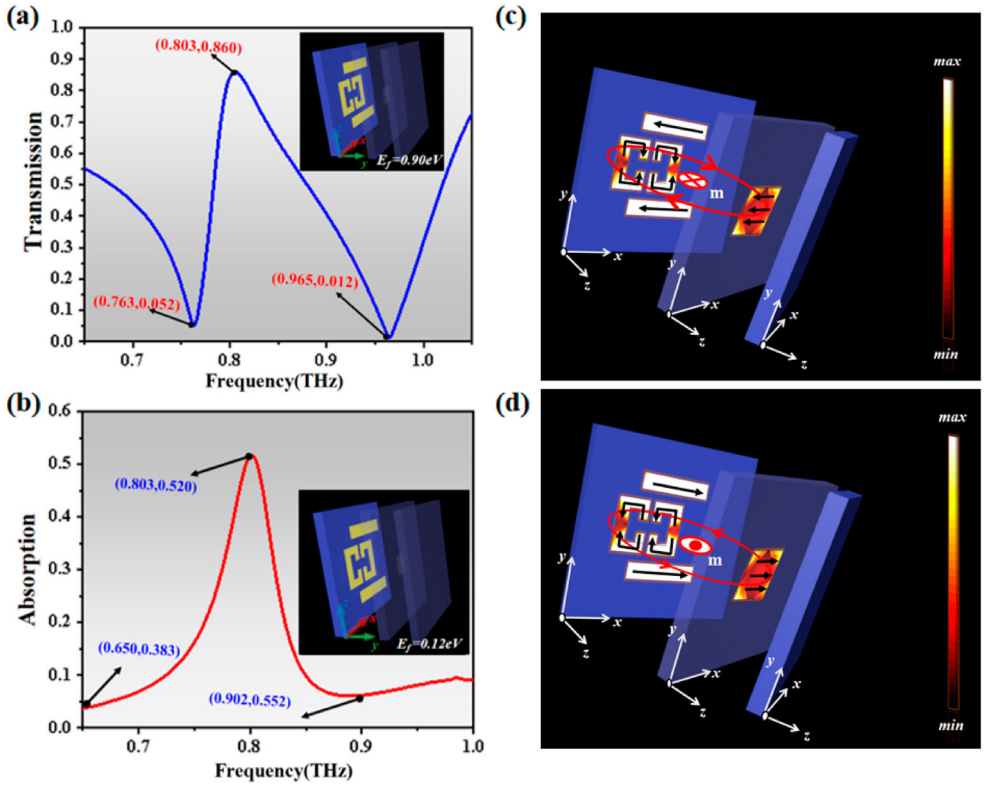

Figure 7. (a) Transmission curve of EIT formed at $E_f = 0.9$ eV, (b) Absorption curve of EIA formed at $E_f = 0.12$ eV, (c,d) Simulated surface current and electric field diagram distribution for the three-layer case where (c) at peak absorption frequency when $\varphi = 0.89\,\pi$, and (d) At peak absorption frequency when $\varphi = 1.89\,\pi$.

attenuate the electromagnetic wave energy, making as much of the electromagnetic wave incident inside the material as possible and reducing the reflection of the electromagnetic wave on the material surface are necessary. For this purpose, a good impedance matching is required. For the conductivity loss, according to the free-electron theory [49], increasing the conductivity can help to enhance the loss, but too high conductivity is not conducive to impedance matching and will cause strong surface reflection.

In addition, absorption is a complex process, and in EIA metastructure, all constituent materials are lossy. And in the high-frequency part, the loss is higher. Therefore all components, i.e. GSP, metal cut wires, two SRRs, and dielectric substrates, all contribute to the absorption of EIA, and its essence is also reflected in the change of the absorption curve. The loss of this structure depends mostly on the GSP, and the conductivity is low when the single-layer graphene E_f is small, but here we set the GSP thickness to 0.1 μm (the standard thickness of single-layer graphene is 0.334 nm) to increase the conductivity at a fixed E_f of graphene. And we calculate the Re (σ) and Imag (σ) of the conductivity of the GSP ($E_f = 0.9$, 0.12 eV) in both states by Kubo's formula. As shown in Figure 8(a) and (b), in the operating frequency range, at 0.12 eV, the conductivity of the GSP is close to 1 S/m. Compared with the high E_f state GSP, the GSP carrier mobility at this time is low, the equivalent impedance is

high, and the dielectric loss is large. The main sources of dielectric loss are as follows: under the action of the electric field, due to the dielectric leakage phenomenon (the actual working dielectric always exists conductivity loss, some weakly connected charged particles in the dielectric under the action of an external electric field can be made along the direction parallel to the electric field for the movement between the electrodes thus generating leakage conductive flow so that the energy is directly lost. Especially at high temperatures or strong electric field, this aspect has a great impact) and the hysteresis effect of dielectric polarization (related to the scattering rate Γ in Equation (3), and high-frequency effect), GSP will consume a lot of energy. This can be understood more intuitively by the equation. The electric field of electromagnetic waves in the GSP produces a conduction current density $J_c = \sigma E$, which causes a power loss that attenuates the amplitude of the electromagnetic waves, and the average value of the power loss time per unit volume is:

$$p = \frac{1}{2}\mathrm{Re}[J_c \cdot E^*] = \frac{1}{2}\sigma {E_m}^2 \tag{9}$$

where E_m is the magnitude of the electric field amplitude on the GSP, and $E*$ refers to the conjugate complex of E. Since the higher the conductivity σ, the lower the impedance and the amplitude E_m decreases, the higher the conductivity is not better, and optimal value needs to be found by parameter optimization. The complex dielectric constant is $\epsilon_\mathrm{c} = \epsilon^{'} - \mathrm{j}\epsilon''$. The displacement current density on the medium is $J_\mathrm{d} = \mathrm{j}\omega\epsilon^{'}E + \omega\epsilon'' E$, where the displacement current component in phase with E also causes power loss, and the time average of the polarization power loss per unit volume of the medium can be expressed as:

$$p = \frac{1}{2}\mathrm{Re}[J_d \cdot E^*] = \frac{1}{2}\omega\varepsilon'' {E_m}^2 \tag{10}$$

It can be seen that the polarization power loss and the imaginary part of the complex dielectric constant make proportional, and the higher the frequency the more likely the hysteresis effect of dielectric polarization, and the greater the polarization loss. The total current on the GSP exceeds the voltage (90-o)°, o is the loss angle, and the loss angle tangent of GSP is:

$$\tan o = |\frac{\varepsilon''}{\varepsilon'}| \tag{11}$$

The magnitude of the loss angle tangent of GSP at a given frequency can be illustrated by the magnitude of the loss of GSP at this frequency. Figure 8(c) shows the tan$o$ of graphene in two states ($E_\mathrm{f} = 0.9, 0.12$ eV) and at 0.12 eV, the tan$o$ of the absorption peak frequency point (0.803 THz) can reach 0.259. It can be seen that the polarization loss of graphene is larger than the contribution of the field due to polarization. It is worth stating that the loss of GSP contributes to EIA, but it is limited due to the small shape of GSP. The largest contribution to trigger the transition from EIT to EIA is the magnetic dipole generated by the interference of the triple resonator configuration, which strongly traps the incident magnetic energy and increases the absorption (as shown in Figure 7), but the higher the conductivity is not better, too high conductivity is not good for impedance matching and causes strong surface reflections. This is the main reason why the transmission peak is obtained at 0.9 eV and the absorption peak at 0.12 eV. Even though the loss is finite, it does contribute to the EIT/EIA conversion, and our original intention in writing this section was to elaborate as much as

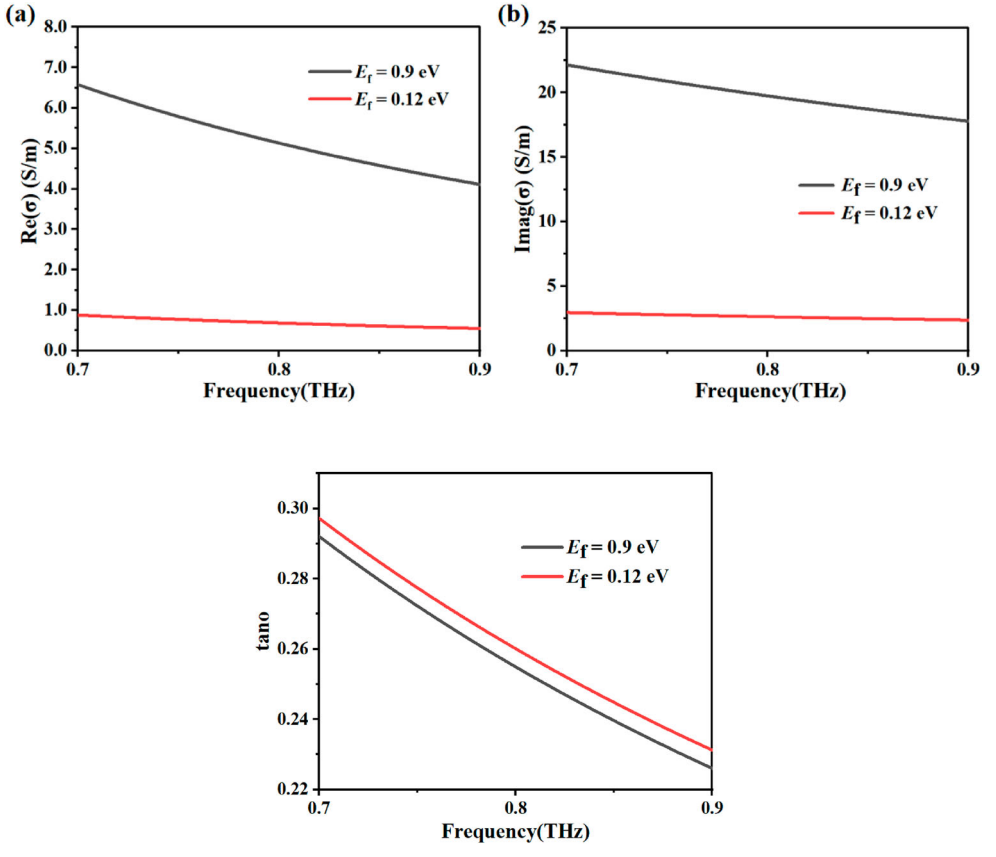

Figure 8. Electromagnetic parameters of GSP in the interval from 0.7 THz to 0.9 THz in two states (E_f = 0.9, 0.12 eV): (a) real part of complex conductivity, (b) imaginary part of complex conductivity, and(c) loss angle tangent.

possible on the various physical mechanisms behind the formation of this phenomenon, so we also discuss it from the loss point of view.

It is known that the change in graphene loss is also accompanied by a change in surface impedance. Li et al. in 2020 [50] designed a polarization-sensitive switchable metamaterial THz device with broadband absorption and modulation properties using the frequency-dependent and surface impedance-related properties of graphene at different E_f. The work is also explained using the impedance matching principle to justify the work. To further verify the physical mechanism behind the EIT to EIA conversion, the impedance matching principle is also introduced here. The equivalent impedance (Z) of the proposed GMST is assumed to be approximately equal to the equivalent impedance (Z_0) in free space, thus improving the absorption of EIA. The normalized complex impedance $Zr = Z/Z_0$ is also introduced to reflect the degree of impedance matching between Z and Z_0 (Zr is 1, when perfect absorption is achieved). In addition, the equation to invert Zr by S-parameters is as follows [3]:

$$Zr = \sqrt{\frac{(1 + S_{11}(\omega))^2 - S_{21}(\omega)^2)}{(1 - S_{11}(\omega))^2 - S_{21}(\omega)^2)}} \tag{12}$$

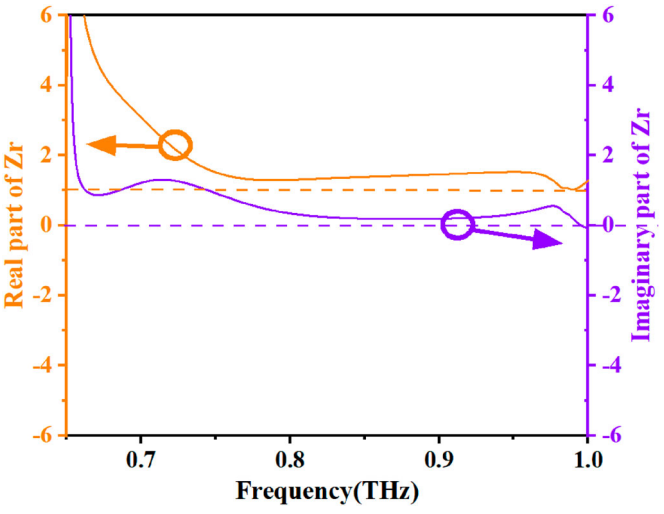

Figure 9. The normalized complex impedance Zr of the GMST at 0.12 eV.

where $S_{11}(\omega)$ and $S_{21}(\omega)$ refer to the scattering parameters of reflection and transmission, respectively. the convergence of the real and imaginary parts of Zr to 1 and 0, respectively, is one of the signs of complete absorption. As shown in Figure 9, the real part of the normalized input impedance of Zr is about 1 and the imaginary part is close to 0 in the EIA operating band of 0.65 $\sim$ 0.9 THz, which proves that the system achieves perfect impedance matching with free space in this band and also indirectly verifies that the surface impedance of GSP at 0.12 eV is the best point for forming EIA.

To explain the formation of the EIA effect, a typical four-energy atomic system shown in Figure 10(a) is introduced, where the EIA phenomenon can be observed in an atomic system driven by coherent coupling effects. Among them, $|1>$ and $|3>$ are simple merged ground state energy levels without relaxation, and $|2>$ and $|4>$ are also simple merged excited state energy levels [48]. Unlike the EIT, not only coupling light and detection light are needed here for coupling and detection of EIA, but also additional control light is needed to realize the jump from energy level $|3>$ to $|4>$ [51]. In Figure 10(a), Ω_1, Ω_2, and Ω_3 are the Rabi frequencies of coupling light, detection light, and control light respectively (when an atom or other two-energy system is irradiated by coherent light, it will periodically absorb photons and re-emit them by excited emission, and the inverse of such a period is called the Rabi frequency), and γ_1, γ_2, γ_3 are the rates of the three leap channels when the states change rate, respectively [52]. In different cases (e.g. the Rabi frequency of the coupling field, the control field, and the decay rate of the fourth simple energy level are not the same), the atomic coherence process of the four-energy atomic system has different effects on the medium absorption, that is, the atomic coherence converts the absorption from phase length interference to phase destructive interference, i.e. from EIT to EIA. As shown in Figure 10(b), the metal cut wires in the metastructure unit structure designed in this paper correspond to the energy level $|1>$ to $|2>$ leap, while the two SRRs represent the energy level $|2>$ to $|3>$ and the GSP corresponds to the energy level $|3>$ to $|4>$ leap, and the GSP and the two SRRs can exchange energy with each other through

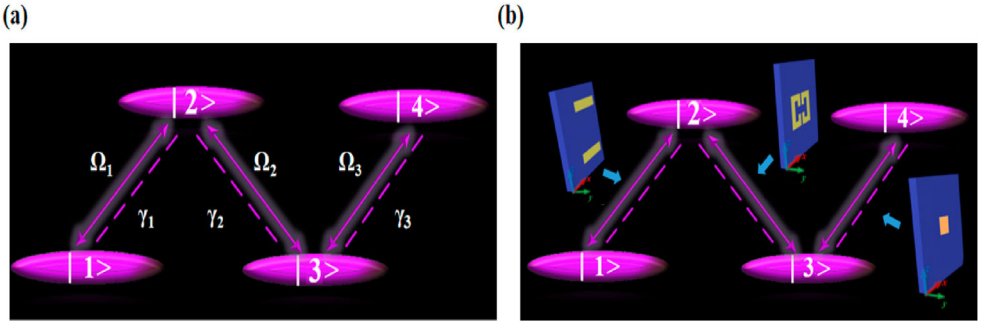

Figure 10. The comparison of the coupling mechanism between: (a) Schematic diagram of electromagnetic induced absorption phenomenon in a four-energy atomic system, and (b) the presented GMST.

near-field coupling, so the metastructure unit structure does not need to control the EIA can be achieved without controlling the corresponding simulation of light.

In order to further analyze the formation mechanism of the transition between EIT and EIA, a coupled two-oscillator model is introduced. Oscillator 1 is used to simulate the cut wires that can be directly excited by the incident field E(t) with a response of x_1(t) and a large decay rate of γ_1. Oscillator 2 is used to represent two SRRs with response x_2(t) and small decay rate γ_2, which can only be driven by oscillator 1 through near-field interactions. If the coupling strength κ is a constant, it is a simple EIT simulation system. Therefore, a complex coupling parameter $\kappa\exp(j\varphi)$ needs to be introduced to fully describe the action of the GSP and thus the complex EIT to EIA system, where the parameter φ expresses the spectral transformation between EIA and EIT. Note that when $\varphi = 0$, the model is only suitable for pure EIT resonances, while if $\varphi = \pi/2$, it is only suitable for pure EIA resonances. To better elucidate the mode interference between the bright and dark resonators, the following coupled differential equations are proposed [53]

$$x_1''(t) + \gamma_1 x_1'(t) + \omega_0^2 x_1(t) + \kappa\exp(j\varphi)x_2(t) = gE(t) \tag{13}$$

$$x_2''(t) + \gamma_2 x_2'(t) + (\omega_0 + \delta)^2 x_2(t) + \kappa\exp(j\varphi)x_1'(t) = 0 \tag{14}$$

Where ω_0 and $(\omega_0+\delta)$ are the resonant angular frequencies of oscillators 1 and 2, respectively. To indicate the coupling efficiency of the dipole mode to the incident electromagnetic field, g is introduced and it is a geometric parameter. Introducing the harmonic ansatz x_1(t) $= a_1\exp(-j\omega t)$, $x_2(t) = a_2\exp(-j\omega t)$ and $E(t) = E_0\,(t)\exp(-j\omega t)$[53], the amplitudes of the bright and dark modes are written as follows [52]:

$$a_1(\omega) = \frac{-gE_0(\omega^2 + j\omega\gamma_2 - (\omega_0 + \delta)^2)}{(\omega^2 + j\omega\gamma_1 - \omega_0^2)(\omega^2 + j\omega\gamma_2 - (\omega_0 + \delta)^2) - k^2\exp(j2\varphi)} \tag{15}$$

$$a_2(\omega) = \frac{gE_0 k\exp(j\varphi)}{(\omega^2 + j\omega\gamma_1 - \omega_0^2)(\omega^2 + j\omega\gamma_2 - (\omega_0 + \delta)^2) - k^2\exp(j2\varphi)} \tag{16}$$

The absorption rates obtained were as follows [53]:

$$A(\omega) = \frac{jg^2\omega(\omega^2 + j\omega\gamma_2 - (\omega_0 + \delta)^2)}{(\omega^2 + j\omega\gamma_1 - \omega_0^2)(\omega^2 + j\omega\gamma_2 - (\omega_0 + \delta)^2) - k^2\exp(j2\varphi)} \tag{17}$$

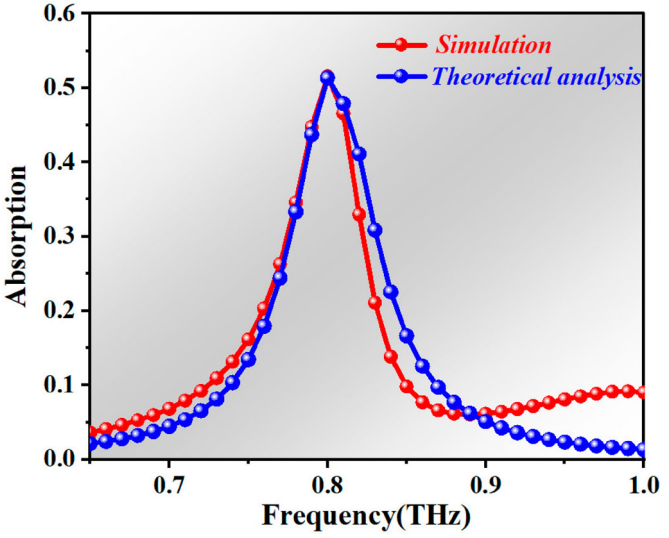

Figure 11. Comparison of the simulated and theoretical absorption curves of the proposed GMST.

With the approximation ${\omega_0}^2 - \omega^2 = -2\omega_0(\omega - \omega_0)$, Equation (17) can be simplified into [53]

$$A(\omega) = \mathrm{Re}\frac{jg^2(\omega - (\omega_0 + \delta) + j\gamma_2/2)}{(\omega - \omega_0 + j\gamma_1/2)(\omega - (\omega_0 + \delta) + j\gamma_2/2) - k^2\exp(j2\varphi)/4} \tag{18}$$

The parameters after fitting through Equation (18) are as follows: $\gamma_1 = 0.4$, $\gamma_2 = 0.01$, $k = 0.004$, $g = 0.322$ in Figure 11. The simulated and theoretical absorbance curves can be regarded as consistent. Some deviations may be due to some losses and complex coupling generated in the design.

3. Results and discussion

3.1. The slow-light effect of the EIT effect

The EIT effect is usually accompanied by a slow light effect due to strong dispersion. In transparent windows, drastic phase changes lead to high group delay (GD), fully demonstrating the significant slow light effect. In addition, the corresponding group index (GI) can describe the slow-wave effect in the proposed GMST. The calculation is as follows [54]

$$\tau_{GD} = -\frac{\partial\varphi}{\partial\omega} \tag{19}$$

$$n_{GI} = \frac{c}{t}\tau_{GD} \tag{20}$$

Where ω, φ c, and t denote the angular frequency, the transmission phase, the light speed in a vacuum, and the total thickness of the proposed GMST, respectively. Therefore, the phase of the incident wave in Figure 12(a) shows two abrupt changes on both sides of the EIT transmission window, which is consistent with the typical EIT and facilitates the emergence of the slow-wave effect. As shown in Figure 12(b), it is clear that when TM mode wave

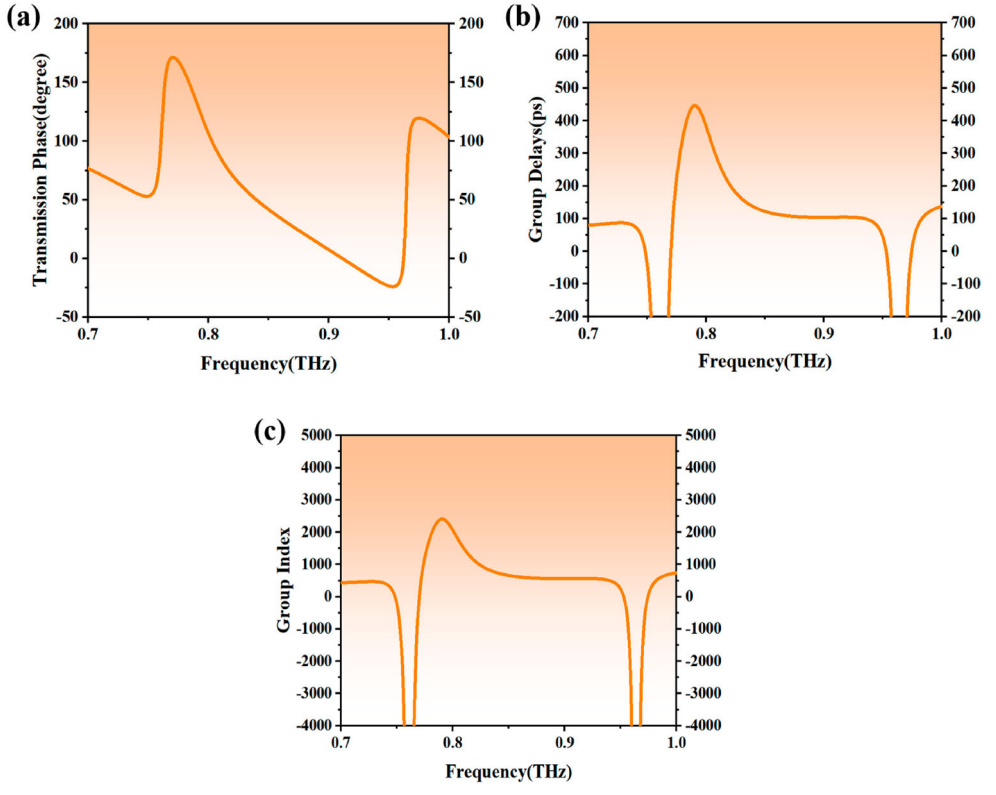

Figure 12. (a) The transmission phase, (b) the group delays, and (c) the group index of the proposed GMST.

incident, the maximum GD value is 447 ps, and the corresponding GI in Figure 12(c) is 2410, showing a significant slow-light effect.

3.2. The adjustability of the EIT and EIA

In addition, the introduction of GSP improves the performance of the GMST, i.e. makes the EIT transmission and EIA absorption adjustable without changing the structure. As shown in Figure 13(a) and (b), when E_f is gradually changed from 0.1 eV, as GSP is located at the top layer of the original two-resonator EIT metastructure, it couples with the underlying EIT metastructure to enhance the generation of strong currents as the GSP conductivity gradually increases. The interaction between the two SRRs and the GSP generates a reverse current, forming a magnetic dipole with the same polarization direction as the incident magnetic field, which strongly traps the incident magnetic energy, thus causing a strong absorption and realizing the conversion from EIT to EIA. At around 0.3 eV of $E_{f,}$ in addition to a significant frequency shift of the transmission window, the EIT to EIA transition reaches its strongest due to the superposition of the constructive interference between the three resonators and good impedance matching. Thereafter, with the increase of E_f, the EIT phenomenon starts to be obvious considering that the GSP carrier mobility becomes higher, the equivalent impedance decreases, the dielectric loss decreases. Moreover, the

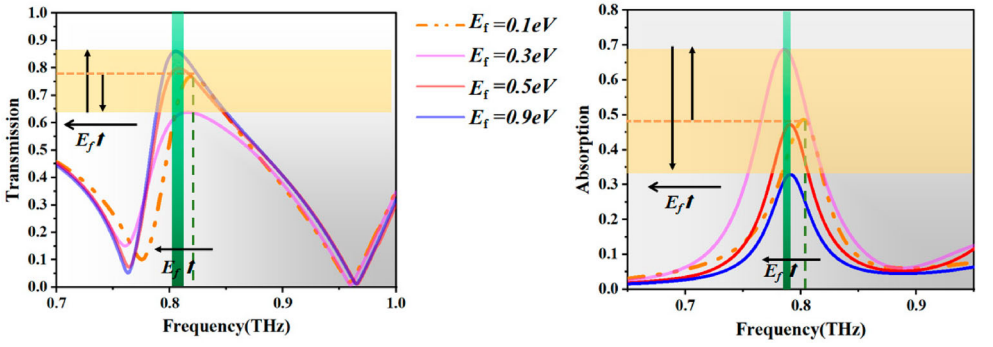

Figure 13. The response of (a) the transmission, and (b) the absorption curves with E_f from 0.1 to 0.9 eV.

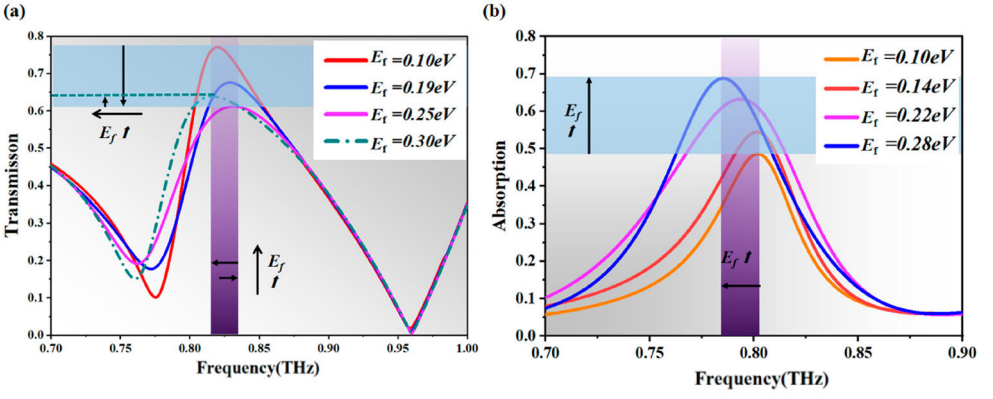

Figure 14. The response of (a) the transmission, and (b) the absorption curves with E_f from 0.1 to 0.3 eV.

impedance matching in space starts to detune and the surface reflection is enhanced. Thus 0.9 and 0.12 eV are chosen as the proposed EIT to EIA GMST, because both the transmission and absorption peaks are larger at this point and the frequencies coincide, both at 0.803 THz. To better visualize the role of GSP, the transmission curves are plotted at 0.1–0.3 eV, as shown in Figure 14(a) and Figure 13(b), where the EIT transmission decreases and then increases with increasing E_f, reaching a minimum at 0.25 eV and a nonlinear frequency shift occurs. And the EIA absorption peak increases with E_f, and both the absorption peak and frequency shift change linearly with increasing E_f in the 0.1–0.3 eV blank section of Figure 14(b).

The absorption response of GMST at different polarization angles is also a noteworthy issue. As shown in Figure 15, when $\alpha < 20°$, the EIA phenomenon is stable, and as the incidence angle increases, the original absorption peak decreases and another absorption peak is formed at high frequencies.

3.3. The structural parameter discussion of the given GMST

Consistently, the use of GSP has been implemented to tune the performance of the GMST. However, to further explore the effect of structural parameters on the performance, the

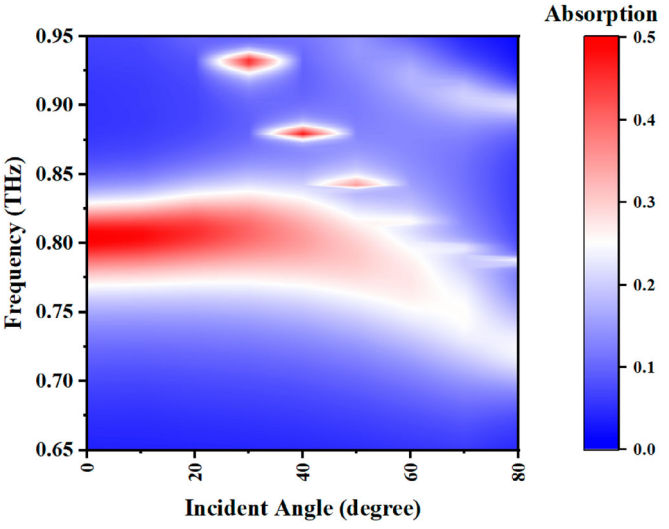

Figure 15. The absorption responses with different polarization angles(α), α is the angle between the electric field and the x-axis when $\alpha = 0°$, the electric field direction is along the x-axis, that is, the TM mode incidence.

critical thickness H_1 of the last layer of the dielectric substrate through which the wave vector passes has been chosen for discussion. Clearly, with the expansion of H_1, the entire EIT and EIA windows are found to exhibit a redshift as shown in Figure 16(a) and (b), and there is almost no change in the transmitted EIT peak. As a beam of electromagnetic waves passes through the material, to effectively attenuate the electromagnetic wave energy, it is necessary to first make as many electromagnetic waves as possible to be incident inside the material and reduce the transmission. For this reason, the thickness of the last layer of the dielectric substrate, H_1, is conducive to achieving good impedance matching. In addition, the atomic system in the EIA is different, the role of ohmic loss needs to be additionally considered, and in the high-frequency part, the greater the loss. The loss part also depends on the thickness of the dielectric substrate, its essence is also reflected in the change of the absorption curve. However, due to the high requirements of the EIT to EIA system for frequency point alignment, here at the expense of EIA peak selected peak frequency point alignment of H_1 of the parameter 15 μm. In addition, the coupling distance H_3 between the GSP and EIT metastructure is also an important parameter. As shown in Figure 16(c) and (d), Clearly, with the expansion of H_1, the entire EIT and EIA windows are found to exhibit a redshift as shown in Figure 16(c) and (d), and there is almost no change in the transmitted EIT peak. At the same time, the absorption peak increases. This is the result of the degree of coupling, in order to meet the peak frequency requirements of the EIT to EIA system, EIA peak was sacrificed and $H_3 = 15$ μm was selected.

Finally, to systematically and visually describe the novelty and impact of this work, we summarize the relevant EIT/EIA devices with superior performance reported in the last three years in Table 2. Multitasking metastructures facilitate the miniaturization of optoelectronic devices for a wide range of applications and tunable devices have flexible applications. In general, the EIT/EIA dual-function metastructures proposed in this work is advanced and valuable compared with the listed research works.

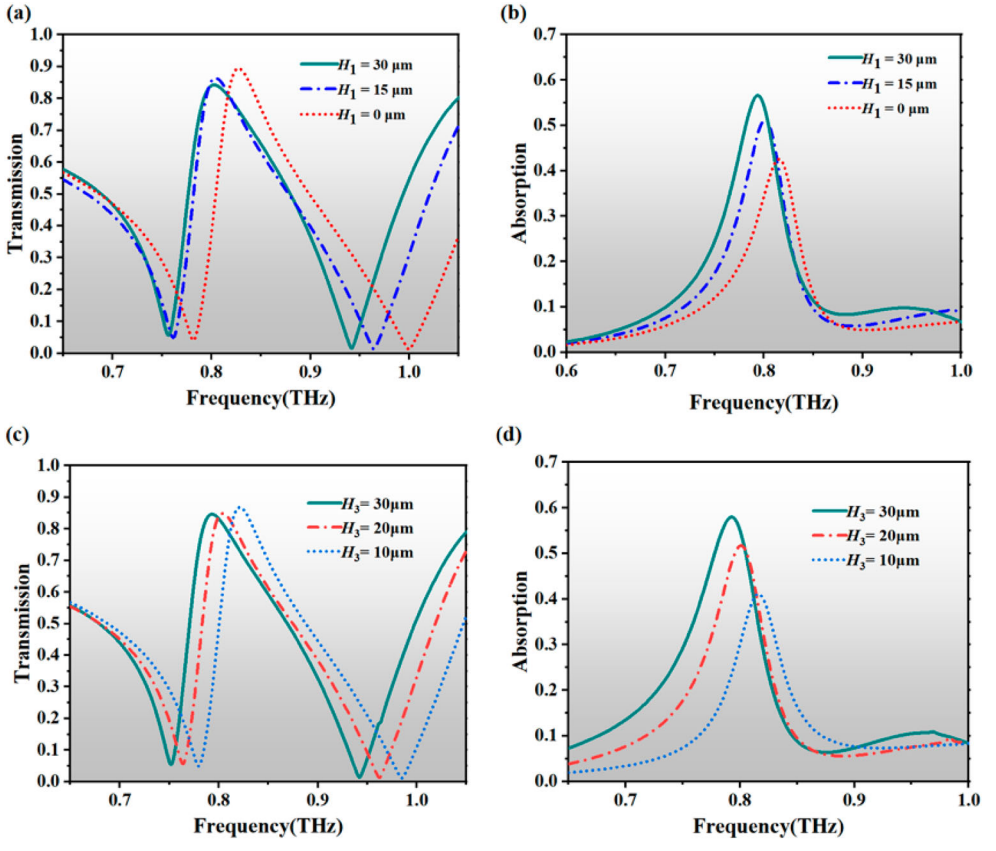

Figure 16. The calculated (a) Transmission curves at 0.9 eV, and (b) Absorption curves at 0.12 eV of the GMST when H_1 varies from 0 μm to 30 μm. The results of (c) Transmission curves at 0.9 eV, and (d) Absorption curves at 0.12 eV when H_3 differs from 10 μm to 30 μm.

Table 2. Comparison of the proposed work with previous work with optical surface technologies.

Ref.	External variables	Active material	Adjustment object	Functionality	Optimum performances and frequencies
[8]	None	None	None	ultra-narrow EIT	0.331 THz: $T_m = 0.87$;
[17]	Voltage	graphene	frequency regions	multiband EIT	8.31 μm: $T_m = \sim 0.98$ ~ 8.37/8.44/8.62 μm: (Ef = 0.60 /0.58/0.56 eV) $T_m = \sim 0.95$
[15]	Voltage	linear shapes	PIN diode	ultra-narrowband EIT	2.97 GHz: $T_m = \sim 0.90$ (Ebias = 1.2 V)
[4]	Temperature	Vanadium Dioxide	Functionality	EIT	1.08 THz: $T_m = \sim 0.43$
				polarization conversion	Relative bandwidth: 29%
[55]	None	None	None	Resonance absorption	2.4 GHz: $A_m = \sim 0.97$
[56]	None	None	None	EIA	15.37 μm: $A_m = \sim 0.76$
This work	Voltage	graphene	Functionality /Amplitude	EIT	0.803 THz: $T_m = \sim 0.86$
				EIA	0.803 THz: $A_m = \sim 0.52$

4. Conclusion

In summary, by using the constructive interference between the three resonators and the characteristics of the GSP conductivity and dielectric loss varying with the E_f, it is possible to realize the GMST from EIT to EIA conversion characteristics in the three-resonator metastructure. When $E_f = 0.9$ eV, the graphene has less influence on the lower EIT metastructure, and the EIT phenomenon of the triple-resonator metastructure is realized. The EIT transmission window appears between 0.763 and 0.965 THz, and at 0.803 THz, the transmission peak reaches 0.860. When $E_f = 0.12$ eV, GSP has a certain conductivity and is weakly coupled to the substructure, thus constructive interference between the three resonators generates a magnetic dipole that strongly traps the incident magnetic energy, thus contributing to the EIA phenomenon. The absorption window appears between 0.650 and 0.902 THz. The frequency point of the absorption peak of the EIA phenomenon at this time coincides perfectly with the frequency point of the transmission peak of EIT at $E_f = 0.9$ eV, both at 0.803 THz. The contribution of the dielectric loss of the GSP itself to the absorption is also qualitatively analyzed. In addition, the working principle of this metastructure is explained through the surface current distribution. To reproduce EIT and EIA, the two-oscillator model is used and the simulation results are proved to be consistent and valid. The structural parameters are also discussed and the properties of the GMST are explored. The GMST proposed in this paper can produce an absorption band in the original EIT transmission window, which opens a new way for advanced information encoding technology, decoding and decoding technology, group velocity modulation technology, and frequency selection technology. We believe that graphene-dielectric metamaterials with hyperbolic response [57] are promising and will work well for EIT to EIA in the future.

Disclosure statement

No potential conflict of interest was reported by the author(s).

Funding

This work was supported by College Student Innovation Training Program of Nanjing University of Posts and Telecommunications.

References

[1] Wang BX, He YH, Lou PC, et al. Design of a dual-band terahertz metamaterial absorber using two identical square patches for sensing application. Nanoscale Adv. 2020;2:763.
[2] Brown ER. Fundamentals of terrestrial millimeter-wave and THz remote sensing. Int J High Speed Electron Syst. 2003;13(04):995–1097.
[3] Sun YZ, Gao CJ, Qu J, et al. Circularly polarized manipulations with VO_2-doped dielectric electromagnetically induced transparency and absorption. Ann Phys. 2022;534(7):2200130.
[4] Gao CJ, Zhang HF. Switchable metasurface with electromagnetically induced transparency and absorption simultaneously realizing circular polarization-insensitive circular-to-linear polarization conversion. Ann Phys. 2022;534(7):2200108.
[5] Wang BX, He YH, Lou PC, et al. Multi-band terahertz superabsorbers based on perforated square-patch metamaterials. Nanoscale Adv. 2021;3:455.
[6] Song Z, Zhu J, Zhu C, et al. Broadband cross polarization converter with unity efficiency for terahertz waves based on anisotropic dielectric meta-reflectarrays. Mater Lett. 2015;159:269–272.

[7] Wang BX, He YH, Lou PC, et al. Miniaturized and actively tunable triple-band terahertz metamaterial absorber using an analogy I-typed resonator. Nanoscale Res Lett. 2022;17:35.
[8] Zhang H, He XC, Zhang D, et al. Multitasking device with switchable and tailored functions of ultra-broadband absorption and polarization conversion. Opt Express. 2022;30(13):23341–23358.
[9] Guo ZH, Sun YZ, Zeng L. Temperature-controlled and photoexcited multitasking Janus metasurface in the terahertz region. Ann Phys. 2022;534(7):2100499.
[10] Wang BX, Xu CY, Zhou HQ, et al. Realization of broadband terahertz metamaterial absorber using an anti-symmetric resonator consisting of two mutually perpendicular metallic strips. APL Mater. 2022;10:050701.
[11] Harris SE, Field JE, Kasapi A. Deceleration of optical pulses based on electromagnetically induced transparency of Rydberg atoms. Phys Rev A. 1992;46:29.
[12] Long F. Wideband and high-efficiency planar chiral structure design for asymmetric transmission and linear polarization conversion. J Appl Phys. 2020;127(2):023104.
[13] Wang BX, Xu W, Wu YK, et al. Multi-band terahertz superabsorbers based on perforated square-patch metamaterials. Nanoscale Adv. 2022;4:1359.
[14] Eisaman MD, André A, Massou F. Electromagnetically induced transparency with tunable single-photon pulses. Nature. 2006;438(7069):837–841.
[15] Gao CJ, Zhang D, Zhang HF. Simultaneously achieving circular-To-linear polarization conversion and electromagnetically induced transparency by utilizing a metasurface. Ann Phys. 2022;534(7):2100578.
[16] Zhang S, Genov DA, Wang Y, et al. Plasmon-Induced transparency in metamaterials. Phys Rev Lett. 2008;101(4):047401.
[17] Zeng C, Cui YD, Liu XM. Tunable multiple phase-coupled plasmon-induced transparencies in graphene metamaterials. Opt Express. 2020;23(1):545–551.
[18] Taubert R, Hentschel M, Kästel J, et al. Classical analog of electromagnetically induced absorption in plasmonics". Nano Lett. 2012;12(3):1367–1371.
[19] Cao G, Li H, Zhan S, et al. Formation and evolution mechanisms of plasmon-induced transparency in MDM waveguide with two stub resonators. Opt Express. 2013;21:9198.
[20] Chen CY, Un IW, Tai NH, et al. Asymmetric coupling between subradiant and superradiant plasmonic resonances and its enhanced sensing performance". Opt Express. 2009;17(17):15372–15380.
[21] Jin XR, Park J, Zheng H, et al. Highly-dispersive transparency at optical frequencies in planar metamaterials based on two-bright-mode coupling. Opt Express. 2011;19(22):21652–21657.
[22] Zhu Y, Hu X, Yang H, et al. On-chip plasmon-induced transparency based on plasmonic coupled nanocavities. Sci Rep. 2014;4:3752.
[23] Amin M, Farhat M, Bagcı H. A dynamically reconfigurable fano metamaterial through graphene tuning for switching and sensing applications. Sci Rep. 2013;3:2105.
[24] Cao MY, Wang TL, Zhang HY, et al. Tunable electromagnetically induced absorption based on graphene. Opt Commun. 2018;413:73–79.
[25] Zhang X, Xu N, Qu K, et al. Electromagnetically induced absorption in a three-resonator metasurface system. Sci Rep. 2015;5(1):10737.
[26] Tassin P, Zhang L, Zhao R, et al. Electromagnetically induced transparency and absorption in metamaterials: the radiating two-oscillator model and its experimental confirmation. Phys Rev Lett. 2012;109(18):187401.
[27] Sen H, Dan L, Hai L, et al. Analogue of ultra-broadband and polarization-independent electromagnetically induced transparency using planar metamaterial. J Appl Phys. 2017;121(12):123103.
[28] Taubert R, Hentschel M, Giessen H. Plasmonic analog of electromagnetically induced absorption: simulations, periments, and coupled oscillator analysis. J Opt Soc Am B. 2013;30(12):3123–3134.
[29] Wan ML, He JN, Song YL, et al. Electromagnetically induced transparency and absorption in plasmonic metasurfaces based on near-field coupling. Phys Lett A. 2015;379(30-31):1791–1795.
[30] Xu N, Manjappa M, Singh R, et al. Tailoring the electromagnetically induced transparency and-absorbance in coupled fano-lorentzian metasurfaces: A classical analog of a four-level tripod quantum system. Adv Opt Mater. 2016;4(8):1179–1185.
[31] Chang S, Mei JS. Active EIT-like dependent on polarization angle with graphene metamaterial. Integr Ferroelectr. 2019;209(1):135.

[32] Ma CW, Ma WY, Tan Y, et al. High Q-factor terahertz metamaterial based on analog of electromagnetically induced transparency and its sensing characteristics. Opto-Electron Eng. 2018;45:180298.
[33] Jabeen M, Haxha S. 2D/3D graphene on h-BN interlayer-silicon solar cell with ZnO:Al buffer layer and enormous light captivation using Au/Ag NPs. Opt Express. 2020;28:12709–12728.
[34] Hansona G W. Dyadic green's functions and guided surface waves for a surfaceconductivity model of graphene. J Appl Phys. 2018;103:064302.
[35] Zeng L, Huang T, Liu GB, et al. A tunable ultra-broadband linear-to-circular polarization converter containing the graphene. Opt Commun. 2019;436(8):7–13.
[36] Huang X, He W, Yang F. Polarization-independent and angle-insensitive broadband absorber with atarget-patterned graphene layer in the terahertz regime. Opt Express. 2018;26(20): 25558–25565.
[37] Yan HG, Li XS, Chandra B. Enhanced optical absorption of graphene by plasmon. Nature Nanotech. 2012;7:330.
[38] Tasolamprou AC, Koulouklidis AD, Daskalaki C, et al. Experimental demonstration of ultrafast THz modulationin a graphene-based thin film absorber through negative photoinduced conductivity. ACS Photonics. 2019;6:720.
[39] Matsumura T, Nakatani T, Yagi T. Production of different types of mannosylerythritol lipids as biosurfactants by the newly isolated yeast strains belonging to the genus Pseudozyma. Appl Phys Lett. 2007;86:107.
[40] Cheng Y, Chen H, Zhao J, et al. Absorbers with spin-selection based on metasurface. Opt Mater Express. 2018;8:1399.
[41] Economou EN. Surface plasmons in thin films. Phys Rev Lett. 1969;182(2):539–554.
[42] Kanté B, Burokur SN, Sellier A, et al. Controlling plasmon hybridization for negative refraction metamaterials. Phys Rev B. 2009;79(7):075121.
[43] Cheng H, Chen S, Yu P, et al. Dynamically tunable plasmonically induced trans-parency in periodically patterned graphene nanostrips. Appl Phys Lett. 2013;103:203112.
[44] Hai L, Dong Y, Song H, et al. Analog electromagnetically induced transparency for circularly polarized wave using three-dimensional chiral metamaterials. Opt Express. 2016;24(26):30068–30078.
[45] Jansen C, Al-Naib I, Born N, et al. Terahertz metasurfaces with high q-factors. Appl Phys Lett. 2011;98(5):2943.
[46] Tassin P, Zhang L, Koschny T, et al. Low-loss metamaterials based on classical electromagnetically induced transparency. Phys Rev Lett. 2009;102(5):053901.
[47] Fedotov VA, Rose M, Prosvirnin SL, et al. Sharp trapped-mode resonances in planar metamaterials with a broken structural symmetry. Phys Rev Lett. 2007;99:147401.
[48] Akulshin AM, Barreiro S, Lezama A. Electromagnetically induced absorption and transparency due to resonant two-field excitation of quasidegenerate levels in Rb vapor. Phys Rev A. 1998;57:2996–3002.
[49] Pan H, Zhang HF. Broadband polarization-insensitive coherent rasorber in terahertz metamaterial with enhanced anapole response and coupled toroidal dipole modes. Adv Opt Mater. 2021;10:2.
[50] Li H, Xu W, Cui Q, et al. Theoretical design of a reconfigurable broadband integrated metamaterial terahertz device. Opt Express. 2020;28(26):40060–40074.
[51] Lezama A, Barreiro S, Akulshin AM. Electromagnetically induced absorption. Phys Rev A. 1999;59:4732–4735.
[52] Taichenachev AV, Tumaikin AM, Yudin VI. Electromagnetically induced absorption in a four-state system. Phys Rev A. 1999;61:011802.
[53] Wan ML, He JN, Song YL, et al. Electromagnetically induced transparency and absorption in plasmonic metasurfaces based on near-field coupling. Phys Rev A. 2015;379:0375–9601.
[54] Lu H, Liu X, Mao D. Plasmonic analog of electromagnetically induced transparency in multinanoresonator coupled waveguide systems. Phys Rev A. 2012;85:053803.
[55] Matsui T, Taniguchi S, Yoshida K, et al. Reflection-less frequency-selective microwave metamaterial absorber. OSA Continuum. 2021;4:2351–2363.

[56] Ruan BX, Liu C, Xiong CX, et al. Absorption and self-calibrated sensing based on tunable fano resonance in a grating coupled graphene/waveguide hybrid structure. J Lightwave Technol. 2021;39:5657–5661.
[57] Hajian H, Caglayan H, Ozbay E. Long-range tamm surface plasmons supported by graphene-dielectric metamaterials. J Appl Phys. 2017;121:033101.